TÜBİTAK

Turkish Journal of Earth Sciences

http://journals.tubitak.gov.tr/earth/

Research Article

Turkish J Earth Sci
(2017) 26: 277-283

doi:10.3906/yer-1706-25

A model for estimating parameters of rotational landslide using a first-order differential equation

Cahit Tağı ÇELİK*
Department of Geomatic Engineering, Faculty of Engineering, Niğde Ömer Halisdemir University, Niğde, Turkey

Received: 28.06.2017 • **Accepted/Published Online:** 11.08.2017 • **Final Version:** 29.09.2017

Abstract: A first-order differential equation was developed and proposed as a search tool in the detection and determination of rotational landslides from two epochs of light detection and ranging (LiDAR) system data in the form of 3D points. To test the proposed method two epochs of LiDAR data were used: one before and one after a rotational landslide occurred. The first epoch of LiDAR data was real, while the second epoch of LiDAR data was simulated based on the first epoch to ensure one or more rotational landslides were included. From the last returns of LiDAR data of both epochs, two functional surfaces were created. Then elevation differences were obtained for identical points in both surfaces. The differenced elevations mainly contain two types of data; one type consists of unchanged elevation differences and the other type includes changed elevation differences. The second type may be considered as outliers with respect to the former. Next, segmentation was performed using the determined outliers. Finally, segmented data were used to estimate the rotational landslide parameters. Using the model, all rotational landslides were detected and their parameters estimated, which were consistent with simulation parameters. In conclusion, the developed model is capable of detecting and determining rotational landslides from 3D data.

Key words: Modelling, first-order differential equations, segmentation, rotational landslides, LiDAR

1. Introduction

Landslide determinations and monitoring are important for understanding their structures and behaviors. Studies for determinations of landslides have utilized a digital terrain model (DTM) created by different sources of data including light detection and ranging (LiDAR), which is a powerful tool to create a bare ground model, canopy model, etc. (Shan and Toth, 2009). Following the creation of the DTM, some terrain analysis is usual for slope, aspect, and curvature models in raster format. Using the results of terrain analysis along with soil parameters, a landslide susceptibility map is created, which is generally based on a single epoch of the DTM (Ostu, 1979; McKean and Roering, 2004; Glenn, et al., 2006; Van Westen, et al., 2008; Shahabi and Hashim, 2015). Remote sensing techniques have been used for detection of landslides by several researchers. Fernández et al. (2008) studied landslide detection in rock masses at Betic Cordilleras, Spain. Two multitemporal epochs of LiDAR data along with supplemental optical satellite imagery were used by Burns et al. (2010) to detect landslides bigger than 0.5 m. A review was done by Jaboyedoff et al. (2012). Chen et al. (2014) proposed a landslide detection procedure in a forested area, involving aspect, slope images, and a DTM. Hastaoğlu (2013) utilized dynamic Kalman filtering in dynamic and kinematic modelling. For a forested area, a landslide susceptibility map was created by Eker and Aydın (2014). For areas of different size, geo-environmental setting, and landslide types, Hussin et al. (2016) proposed a landslide susceptibility model based on weights-of-evidence (WoE). The majority of the studies described above used pixel-based procedures for one epoch of data. However, two epochs of 3D data (one before and after the landslide occurred) may reveal more realistic results for elevation change in topography (Burns et al., 2010). Consequently, modeling them can help one to determine realistic results for landslide determination. One type of landslide is a rotational landslide classified by Varnes (1978). In this field, more modeling for detection and estimation of landslides is needed.

In the present study, a first-order differential equation that governs a rotational landslide is developed and proposed as a search tool in detecting and determining the parameters of rotational landslides from two epochs of LiDAR data: one before and one after a rotational landslide occurred.

* Correspondence: ctcelik@ohu.edu.tr

This study presents some novelties as follows: a) a model for estimation of parameters of rotational landslides is proposed based on first-order differential equations, b) it presents itself as a tool for detection of rotational landslides, c) the proposed procedure is different from others in dealing with vector data (in the form of 3-dimensional coordinates) as opposed to pixel values, d) this approach deals with the subject from the view of deformations.

2. Materials and methods

In this section, model development is given first, then the proposed model is implemented, and finally a description of the data is given.

2.1. Model development

Surfaces may be represented in implicit form as at time t_1 and at time t_2 before and after a rotational landslide has occurred, respectively. When elevation differences of these surfaces are taken, the resulting function can be written as

$$f(x,y)=h_2(x,y)-h_1(x,y), \quad (1)$$

where

$$f(x,y)=\begin{cases} 0 & \text{if there is no change in elevation between } t_2-t_1 \\ f(x,y) & \text{if there are changes in elevation between } t_2-t_1 \end{cases}$$

A rotational landslide classified by Varnes (1978) is shown in Figure 1; it gives an insight into what the difference function *f (x, y)* could be for a meaningful elevation change. The profile AA' represents only the part of in Figure 1, where there are changes in elevations.

A function of the elevation differences between time t_2 and t_1 approximates the final state (Figure 2).

The blue line represents simple elevation difference and the red curve represents best-fit sinus function to the simple difference, respectively, as shown in Figure 2. An elevation-differenced surface can be subdivided into profiles consisting of discrete points with a reasonable width along the steepest slope direction (Figure 3a).

Then each profile (Figure 3a), which may or may not contain points whose elevations changed due to a rotational landslide, may be represented by an approximate piecewise function considering Figure 3b as

$$f^p=f(x,y)=\begin{cases} f(x,y)=0 & \text{if there is no elevation changes} \\ a\times\sin(s_{in\ angle}+b)) & \text{if a rotational landslide occured} \end{cases}, \quad (2)$$

where f^p represents elevations differences of points whose horizontal coordinates are on a *pth* profile. Simple differences of the elevations may be written considering Figures 3a and 3b as

$$h_2(x,y)-h_1(x,y)=a\times\sin(s_{in\ angle}+b),\ \ s_{in\ angle}=\sqrt{x^2+y^2} \quad (3)$$

Eq. (3) can be rewritten in difference equation form as

$$\frac{h_2(x,y)-h_1(x,y)}{\Delta t}=\frac{a\times\sin(s_{in\ angle}+b)}{\Delta t} \quad (4)$$

$$h'(x,y)=\frac{a\times\sin(s_{in\ angle}+b)}{\Delta t}, \quad (5)$$

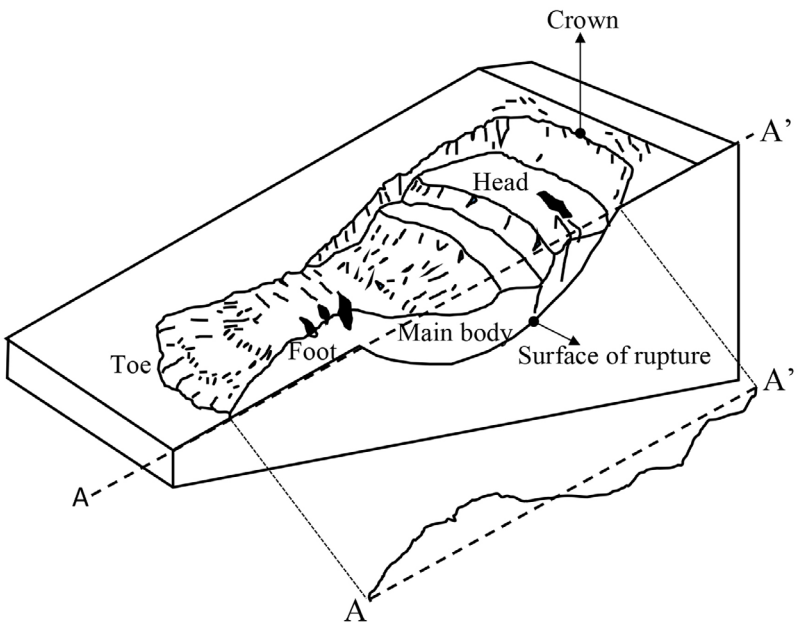

Figure 1. A typical rotational landslide (Varnes, 1978).

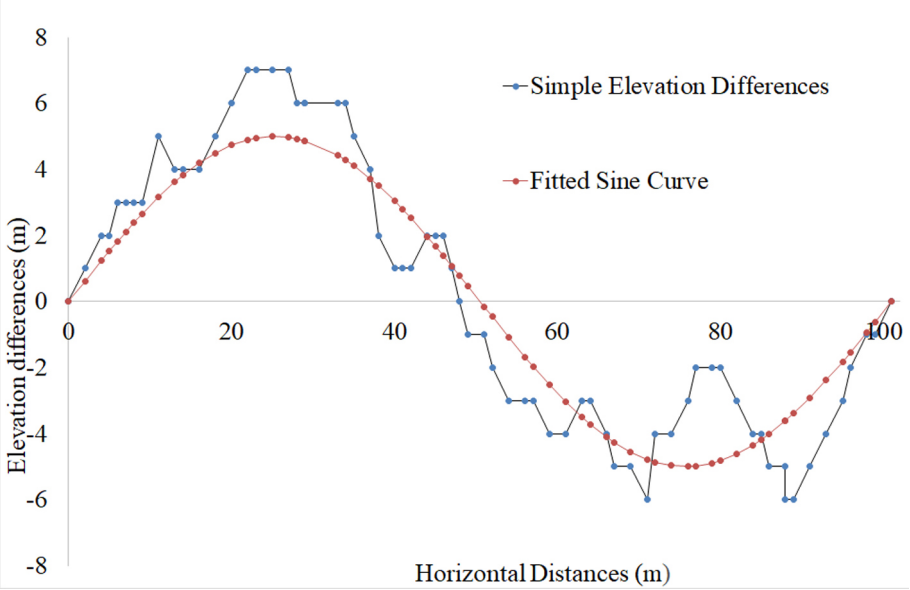

Figure 2. Elevation differences of a rotational landslide and best-fit sinus curve.

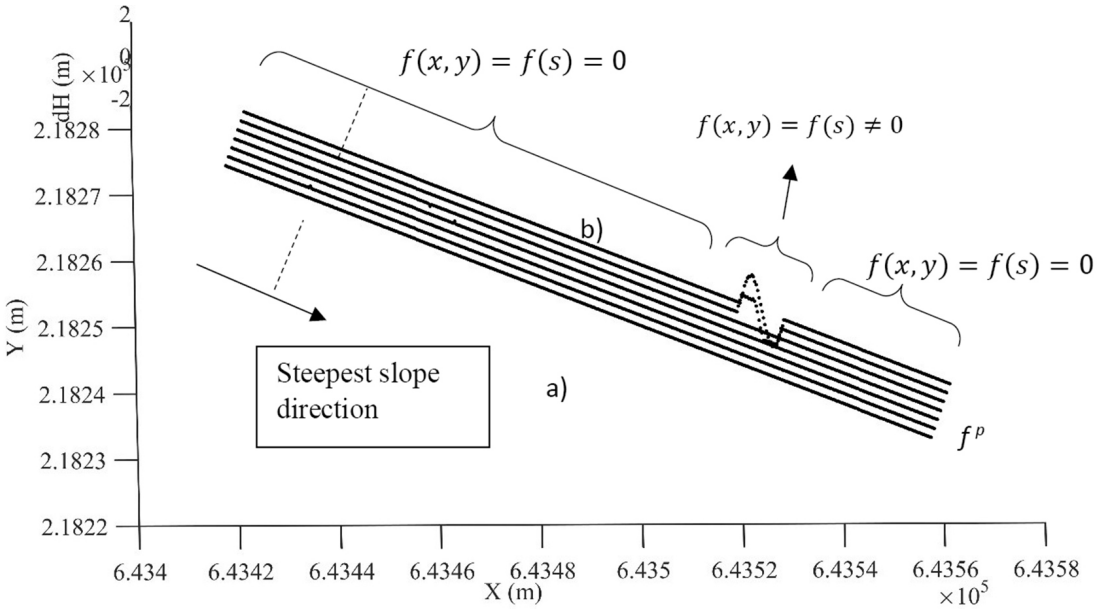

Figure 3. A profiled elevation differenced surface (a) (lower) and two profiles with rotational landslide (b) (upper).

where is an instant of time and therefore considered as unity. Then a first-order differential equation is produced as

$$h'(x,y) = a \times sin(s_{in\ angle} + b), \quad (6)$$

where a is a maximum depletion height of a rotational landslide serving as the amplitude of a sinus function and s is the normalized distance to fit into a 2π period along the steepest slope direction of a particular profile and b is a phase angle. It is noted here that the sin function may include a frequency parameter, but only one cycle of the sinus function is considered, which may represent different movements; therefore it is not considered in this problem.

The left-hand side of Eq. (6) is a derivative with an independent variable time, t, while the right-hand side with an independent variable distance, s. That is a first-order differential equation with unit coefficient of h (t) subject to the initial condition with elevation values of points along a profile in the region. The integral form of Eq. (6) is given by

$$\int dh = \int a \times sin(s_{in\ angle} + b) \times dt \quad (7)$$

$$h = a \times t \times sin(s_{in\ angle} + b) + c\ , \quad (8)$$

where t is an independent variable (time), which may be understood as a unit value due to most landslides not being a slow process with respect to time, that is an instant of time.

Eq. (8) is a general solution to the first-order differential equation, and the integration constant c may be approximately taken as . Here the slope is the one calculated along the steepest slope direction. For the second epoch the equation is given by

$$h^p(x,y) = a \times t_2 \times sin(s_{in\ angle} + b) + slope \times s$$

$$p\ is\ p^{th}\ profile\ at\ time\ t_2 \quad (9)$$

Finally, the solution can be written in terms of the difference of both epochs as

$$f(x,y) = a \times sin(s_{in\ angle} + b) \quad (10)$$

The parameters a and b can be estimated by a least square technique. Eq. (10) may be a useful tool for the detection and determination of the parameters of rotational landslides.

2.2. Implementation of the proposed model

To implement the proposed model, two surfaces were created using the last return of LiDAR data: one before and one after a rotational landslide occurred. Then profile the surfaces along the steepest slope direction. Next, take the elevation differences of identical points in each profile and use these profiles to determine outliers in elevation differences by drawing a box plot, which reveals outlying height differences with 95% confidence. Then impose a condition in each profile whether the elevation differences obey sin waveform, which does not require the value of the parameters in Eq. (10) at this stage of segmentation. This condition searches a number of successive positive elevation differences followed by a number of successive negative elevation differences. This process can group them and distinguish each profile obeying the sin waveform from others. Introduction of this technique was given by Celik (2016). Finally, each group is used to estimate the values of the parameters a, and b using the proposed model (Eq. (10)).

2.3. Description of LiDAR data

The data used in this study were of two types, real LiDAR data and simulated LiDAR data. The real LiDAR data were collected by the Ohio Department of Transportation (ODOT) in 2008 North Zenesville, Ohio, the data of which are based on the NAD HARN State Plane Coordinate System for Ohio South Zone FIPS 3402 converted to meters. An estimated resolution of the LiDAR data was 50 cm. Point spacing was determined as 2.91, which is a number obtained by the total area covered by LiDAR data divided by the total number of points. Estimated horizontal location and vertical accuracies were 9–15 cm and 15–25 cm, respectively. The second type of data was simulated based on the real LiDAR data. In the prepared set, three rotational landslides were inserted having the sizes of 6 × 9 m, 7.5 × 12 m, and 6 × 10.5 m with 2D landslide deposit aspect ratio (amplitude) 11%, 12.5%, and 11.8%, respectively.

3. Results and discussion

A box plot of elevation differenced data is given in Figure 4. Here there are two horizontal lines following the narrow rectangular box in the middle. The points located above and below the two lines were considered outliers (red ones), which refer to the moved points.

This approach is robust to outliers due to the interquartile range used as a confidence interval. For 95% confidence level, the interquartile range is multiplied by 1.5. By taking the outlying points (or deformed points), the area was segmented and three significant rotational landslides were detected (Figure 5) and their locations are plotted in Figure 6.

This robust approach in segmentation was found to be successful in determining the rotational landslides. However, the steepest slope direction is very important for the approach to be successful. If the direction of the rotational landslide is not coincided with the steepest slope direction, then this approach may be used for a preliminary search for possible landslides and then the slope direction is re-determined and applied for the region for proper determination. The positions of simulated

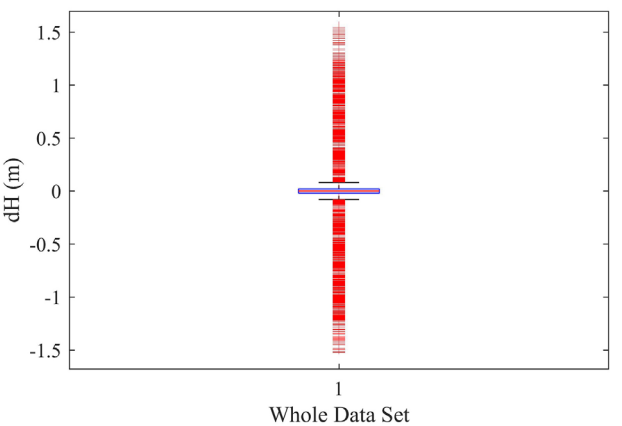

Figure 4. Box plot of elevation differenced data.

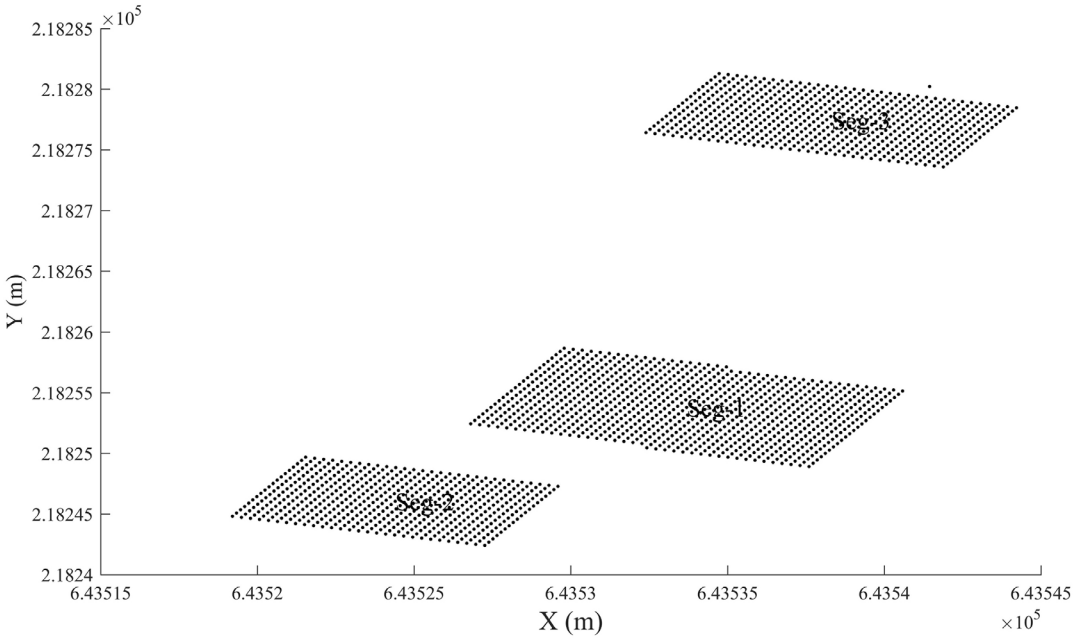

Figure 5. Segmentation results.

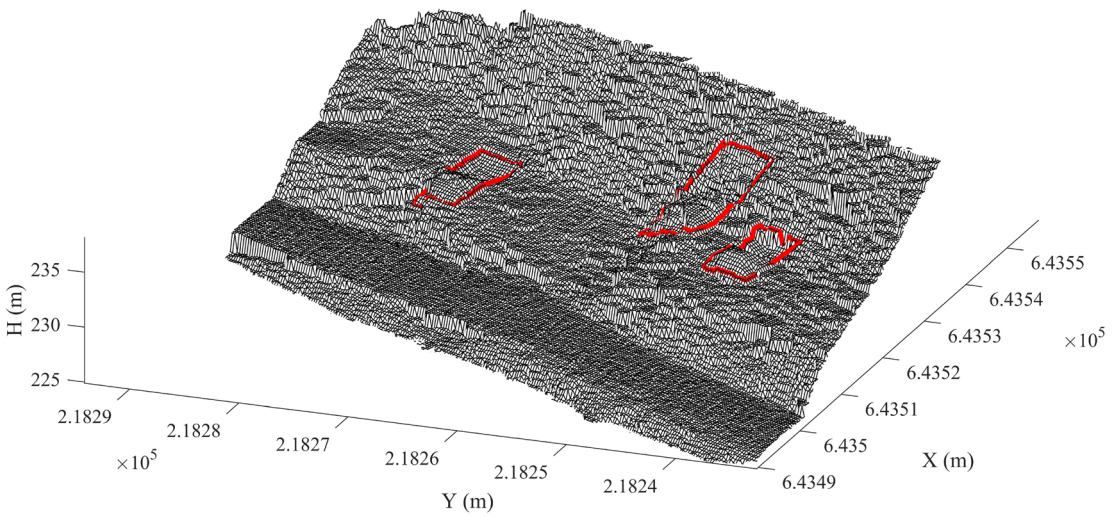

Figure 6. Locations of three rotational landslides.

landslides were selected on purpose to evaluate the approach for rotational landslides that shadow each other from the profiling point of view. This is important in the assessment of the segmentation as recommended by Celik (2016). It is important to stress here that this approach uses point data in 3-D vector format, which differs from the conventional techniques based on raster data.

The proposed model described above (through Eqs. (1)–(10)) was applied to the segmented data and the results are plotted in Figures 7a–7c, correspondingly. Dots represent elevation differences and solid curves represent model outputs. The horizontal axis was formed by normalizing the distance range to fit into the 2π period. Three rotational landslides were detected. For each rotational landslide, the median of the estimated sinus waves for each landslide was taken as the representative of them, which is the bold blue solid curve in Figure 7.

Sizes and amplitudes of landslides of simulated and estimated rotational landslides are tabulated in the Table. The estimated amplitudes of three rotational landslides were 1.07 m, 1.55 m, and 1.22 m, while the simulated values were 1.0 m, 1.5 m, and 1.22 m, respectively. Differences

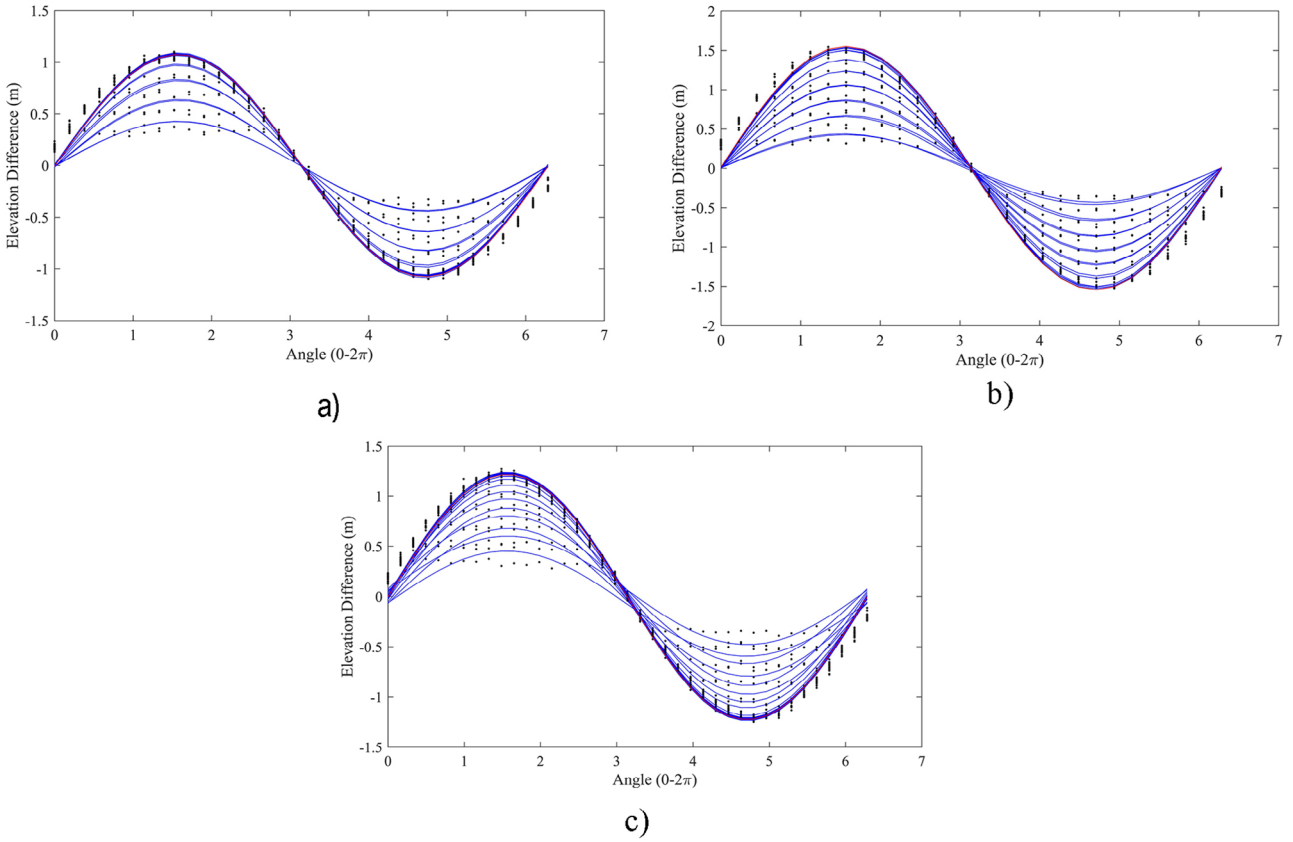

Figure 7. Fitted sinus curve to each segmented area a, b, and c. Here angles represent corresponding s distances normalized to fit into 0–2π.

Table. Simulated and estimated rotational landslide parameters.

Parameter names		a (m)	b (m)	Sigma (m)	Landslide sizes (width × length) (m × m)
Landslide 1	Estimated	1.07	-0.006	0.1	5.7 × 8.7
	Simulated	1.05	0	-	6 × 9
Landslide 2	Estimated	1.55	0.007	0.15	7.2 × 11.7
	Simulated	1.5	0	-	7.5 × 12
Landslide 3	Estimated	1.22	0.002	0.09	5.7 × 10.2
	Simulated	1.2	0	-	6.0 × 10.5

between simulated and estimated amplitudes are due to the white noise added after simulation. The estimated sizes of landslides differ 0.3 m in both width and length, i.e. the size of one grid space.

This is caused by the specified confidence interval for detecting outliers. Estimated phase angles were close to zero, and standards errors were 0.1 m throughout, which indicates that the estimation of fitted curves was properly performed.

4. Conclusions

A model using first-order differential equations for determining parameters of rotational landslides was developed and proposed as a tool for detecting and determining of rotational landslides from two epochs of LiDAR data; the first epoch is real and the second epoch simulated to make sure that one or more rotational landslides are included.

The results of segmentation based on the proposed model were found to be successful in determining each rotational landslide. Using the model their parameters were estimated, and they are consistent with the original simulated parameters. The results indicated that the proposed model is capable of determining and estimating rotational landslides from 3D data.

However, this approach is strongly dependent on steepest slope direction. Amplitude estimation was accurate while size estimation of rotational landslides was one grid length less in both directions than the simulated ones. Another point to make is that the results were obtained from simulated data. Therefore, real data for both epochs should be used to test the proposed model. The proposed model is for estimating the parameters of rotational landslide only. The author recommends studying other types of landslides as well.

Acknowledgment
The author would like to thank the Ohio Department of Transportation for providing data.

References

Burns WJ, Jeffrey AC, Kaya E, Lina MA (2010). Analysis of elevation changes detected from multi-temporal LiDAR surveys in forested landslide terrain in western Oregon. Environ Eng Geosci 16: 315-341.

Celik CT (2016). A robust approach for determining rotational landslide area from two epochs of LiDAR data. 16th SGEM GeoConference on Informatics, Geodesy and Mine Surveying, Geoinformatics and Remote Sensing, Bulgaria, June, Book 2, Vol. 2. pp. 33-38.

Chen W, Li X, Wang Y, Chen G, Liu S (2014). Forested landslide detection using LiDAR data and the random forest algorithm: a case study of the Three Gorges, China. Remote Sens Environ 152: 291-301.

Eker R, Aydın A (2014). Assessment of forest road conditions in terms of landslide susceptibility: a case study in Yığılca Forest Directorate (Turkey). Turk J Agric For 38: 281-290.

Fernández T, Jiménez J, Fernández P, El Hamdouni R, Cardenal FJ, Delgado J, Irigaray C, Chacón J (2008). Automatic detection of landslide features with remote sensing techniques in the Betic Cordilleras (Granada, Southern Spain). Int Soc Photogramme 37, Part B8, 351-356.

Glenn NF, Streutker DR, Chadwick DJ, Thackray GD, Dorsch SJ (2006). Analysis of LiDAR-derived topographic information for characterizing and differentiating landslide morphology and activity. Geomorphology 73: 131-148.

Hastaoğlu KÖ (2013). Investigation of the groundwater effect on slow-motion landslides by using dynamic Kalman filtering method with GPS: Koyulhisar town center. Turkish J Earth Sci 22: 1033-1046.

Hussin HY, Zumpano V, Reichenbach P, Sterlacchini S, Micu M, Westen CV, Bălteanu D (2016). Different landslide sampling strategies in a grid-based bi-variate statistical susceptibility model. Geomorphology 253: 508-523.

Jaboyedoff M, Oppikofer T, Abellan A, Derron MH, Loye A, Metzger R, Pedrazzini A (2012). Use of LIDAR in landslide investigations: a review. Nat Hazards 61: 5-28.

McKean J, Roering J (2004). Objective landslide detection and surface morphology mapping using high-resolution airborne laser altimetry. Geomorphology 57: 331-351.

Otsu N (1979). A threshold selection method from gray-level histograms. IEEE T Syst Man Cybern Syst 9: 62-66.

Shahabi H, Hashim M (2015). Landslide susceptibility mapping using GIS-based statistical models and remote sensing data in tropical environment. Sci Rep 5: 9899.

Shan J, Toth CK (2009). Topographic Laser Ranging and Scanning Principles and Processing. Boca Raton, FL, USA: CRC Press.

Van Westen C, Castellonos E, Kuriakose SL (2008). Spatial data for landslide susceptibility, hazard, and vulnerability assessment: an overview. Eng Geol 102: 112-131.

Varnes DJ (1978). Slope Movement Types and Processes. In: Schuster RL, Krizek RJ, editors. Landslides: Analysis and Control. Transportation and Road Research Board, National Academy of Science, Special Report 176, Washington D. C., pp. 11-33.